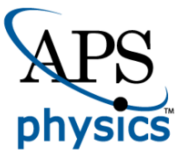

Mid-infrared Optics Using Dielectrics with Refractive Indices Below Unity

Alireza Shahsafi, Yuzhe Xiao, Jad Salman, Bradley S. Gundlach, Chenghao Wan, Patrick J. Roney, and Mikhail A. Kats

Phys. Rev. Applied **10**, 034019 — Published 11 September 2018

DOI: 10.1103/PhysRevApplied.10.034019

Mid-infrared optics using dielectrics with refractive indices below unity

Alireza Shahsafi[1], Yuzhe Xiao[1], Jad Salman[1], Bradley S. Gundlach[1], Chenghao Wan[1, 2], Patrick J. Roney[1], Mikhail A. Kats[1, 2, 3]

[1]Department of Electrical and Computer Engineering, University of Wisconsin-Madison

[2]Materials Science and Engineering, University of Wisconsin-Madison

[3]Department of Physics, University of Wisconsin - Madison

Abstract

Conventional transparent materials at optical frequencies have refractive index values (n) greater than unity—most commonly between about 1 and 4. This paper explores optical phenomena made possible by using materials with refractive indices less than unity. We focus primarily on fused silica (SiO_2), a well-studied dielectric with strong optical-phonon resonances in the mid infrared that result in a spectral region in which $n < 1$ with modest optical loss. Using this ubiquitous easy-to-deposit material, we demonstrate infrared-frequency external reflection, frustrated external reflection, and direct coupling to surface plasmon polaritons from free space. Our work suggests that materials with refractive indices below unity can bring significant new functionalities to optical devices.

1. Introduction

Traditional refractive optical components (*e.g.,* lenses) are made from materials that are transparent in the spectral regions for which they are designed, and typically have refractive indices (n) between 1 and 4 [1]. In such regions, these materials are devoid of optical resonances, resulting in negligible optical losses. Recently, the use of both intrinsic and engineered resonances has enabled the demonstration of a number of exotic optical phenomena, especially in the field of metamaterials [2]. For example, resonances in both the permittivity, ϵ, and permeability, μ, can result in a negative index of refraction ($n = \sqrt{\epsilon\mu} < 0$) [3]–[5]. Similarly, by using electric or magnetic resonances, the values of ϵ or μ can be made to approach zero (*i.e.,* "epsilon-near-zero", or "mu-near-zero", respectively), resulting in a near-zero refractive index ($n \sim 0$) [6], [7]. In such a material, light can propagate without accumulating phase, enabling unique phenomena such as super-coupling [8]. Unfortunately, in many instances, the promise of these exotic phenomena and applications is tempered by optical losses, which are enhanced in close proximity to resonances [9], [10].

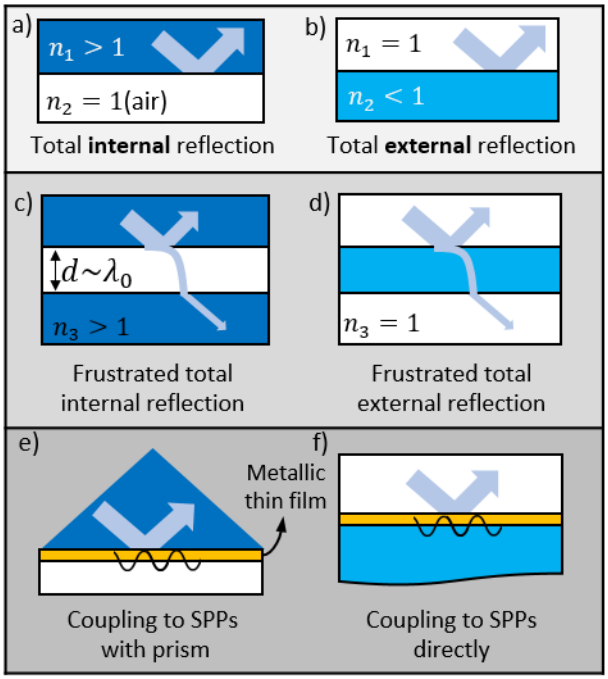

Figure 1) Three well-known optical phenomena (left), and their less-conventional counterparts enabled by materials with $n < 1$ (right)

(a) Total reflection for light incident from a high-index region (1) to air (2), and **(b)** from air (1) to a low-index region (2). **(c-d)** If the thickness of region 2 is comparable to the wavelength of light, λ_0, and a higher-index region 3 is introduced below, some light can be transmitted. This is referred to as frustrated total internal reflection if $n_1 > 1$; by analogy, we refer to the case when $n_1 = 1$ as frustrated total *external* reflection. **(e)** Conventional prism coupling to surface plasmon

polaritons (SPPs), known as the Kreschmann configuration. **(f)** Coupling to SPPs on the interface between metal and a material with $n < 1$ can be achieved with no prism or surface modulation.

In this work, we explore optical phenomena within a spectral range that is close — but not too close — to strong optically active resonances, resulting in the reduction of the real part of the refractive index to below that of vacuum (*i.e.*, $0 < n < 1$). Our demonstrations use a simple homogeneous material, fused silica (SiO_2), which has strong optical-phonon resonances in the mid infrared [11], but is transparent in the visible and near infrared. The intermediate proximity to these optical-phonon resonances results in only a modest increase in the losses, quantified by a small imaginary part of the refractive index, κ. By utilizing the reduction of refractive index in SiO_2 to below one in a portion of the long-wave infrared region, we experimentally demonstrate several unusual optical phenomena, including external reflection (Fig. 1b) and its frustration (Fig. 1d), and direct coupling to surface-plasmon polaritons without the use of prisms or surface modulation (Fig. 1f).

Optical properties of SiO_2

Optical-phonon resonances of dielectric materials such as SiO_2 or aluminum oxide (Al_2O_3) typically lie in the mid-infrared spectral range. The resulting optical properties can be described by Lorentz [12], Gaussian [13], or similar oscillator models and, in the vicinity of such resonances, the refractive index can be below unity [11].

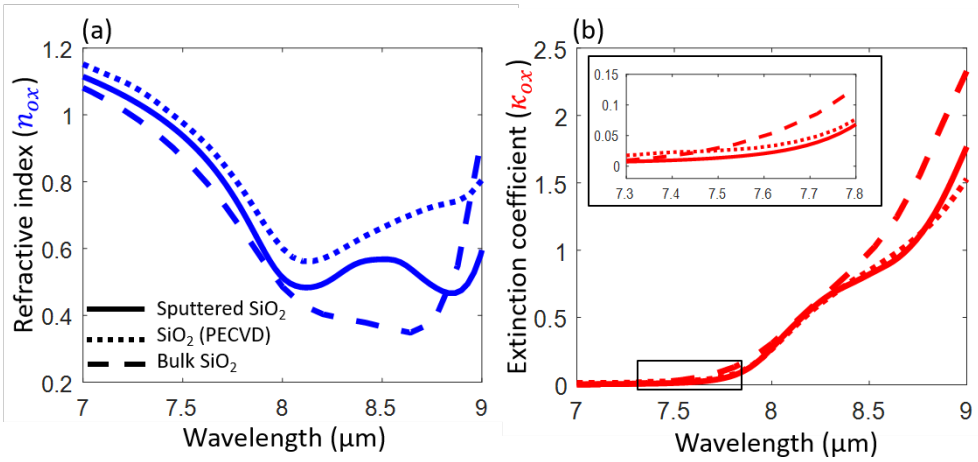

Figure 2) Optical properties of SiO_2

(a) Real (n_{ox}) and **(b)** imaginary (κ_{ox}) parts of the complex refractive index of fused silica (SiO_2) close to its phonon resonances. Two sets of experimentally obtained refractive indices are presented: one of a film grown via plasma-enhanced chemical vapor deposition (PECVD, dotted), and the other from an SiO_2 wafer. For comparison, data taken from ref. [11] are shown using solid lines. Inset: zoomed-in plot of κ_{ox} in a region where $n_{ox} < 1$ and the losses are relatively small.

In this study, we used two types of SiO_2 for the various experiments: thin films grown via plasma-enhanced chemical vapor deposition (PECVD) on high-resistivity silicon, and bulk SiO_2 wafers. The measured refractive index, n_{ox}, and extinction coefficient, κ_{ox}, of these are shown in the Fig. 2 (see section 1 of Supplementary Materials [14] for more details of derived SiO_2 optical properties), and compared to literature data [11]. Though the optical properties differ somewhat between the different samples, in all cases κ_{ox} is relatively small as n_{ox} approaches 1. Specifically, in the 7.3 ~ 7.7 μm region, $n_{ox} < 1$ and $\kappa_{ox} < 0.05$.

2. Results

2.1. Greater reflection than noble metals

When light is incident on a low-index (n_2) material from a high-index (n_1) material, total internal reflection (TIR) occurs for incident angles greater than the critical angle ($\theta_{cr} = \arcsin(n_2/n_1)$) (Fig. 1a). In TIR, the incident medium is usually an optically dense material such as glass. Analogously, when the incident medium is air, and the second material has $n < 1$, a similar phenomenon occurs, referred to as total external reflection (TER). TER is well-known at X-ray frequencies, where complex refractive indices are often written in the form: $\tilde{n} = 1 - \Delta + i\beta$, where typically $\Delta \sim 10^{-5}$ and $\beta \sim 10^{-7}$ [15]. Mirrors based on TER are used for X-ray focusing and other applications [16], [17], and air-core waveguides using TER have been explored theoretically [18].

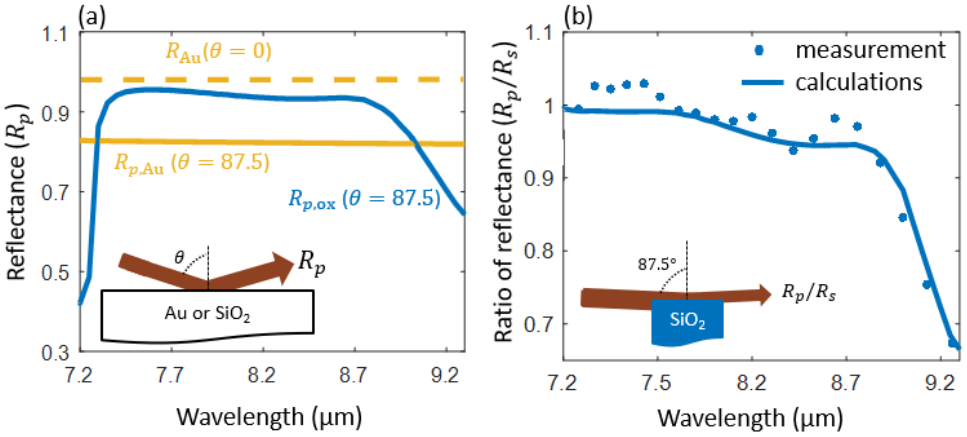

Figure 3) Oblique-angle reflection of SiO_2 can surpass that of gold

(a) Calculated p-polarized reflectance spectra for gold (dashed and solid yellow for normal and oblique incidence, respectively) and an SiO_2 wafer (blue) for incident light coming from air. At large incident angles ($\theta = 87.5°$), the p-polarized reflectance of gold and other metals is suppressed due to the pseudo-Brewster effect. In the wavelength range in which SiO_2 has lower refractive index than unity, the high-angle reflectance of SiO_2 is above that of gold due to external reflection. **(b)** Calculated (solid line) and experimental (circles) ratio of the p- and s-polarized reflectance spectra for our SiO_2 wafer at $\theta = 87.5°$.

In the mid infrared, metallic mirrors can have reflectances of ~ 99% [19], and are often used as references for reflectance measurements. However, for very oblique incidence angles and p polarization, even gold and silver mirrors have a reduced reflectance due to the pseudo-Brewster effect [20], [21] (more discussion in section 2 of Supplementary Materials [14] for further calculation regarding pseudo-Brewster angle). Polished gold mirrors, for example, have significantly decreased reflectance at angles of incidence between 80° and 89° in the near to mid infrared (*e.g.*, Fig. 3a). By comparison, due to TER, materials with $n < 1$ can be used to achieve much larger p-polarized reflectance for these highly oblique angles. We calculated and measured the p-polarized reflectance of an SiO_2 wafer at an incident angle of 87.5° (Fig. 3), and found reflectance values of ~95%, compared to ~82% for gold for $\lambda_0 = 7.3 \sim 8.7\,\mu$m; the SiO_2 p-polarized reflectance is higher than that of gold for angles > 85° (more information in section 2 of Supplementary Materials [14]). We note that due to the highly oblique angle of incidence and relatively small sample area, we were not able to accurately measure the absolute reflectance, because the beam cross section was larger than our sample (see Fig. 3b inset). Instead, we measured the ratio of p-polarized and s-polarized reflectance, eliminating the need for a reference (Fig. 3b). This figure shows good agreement between the measurement and calculations based on Fresnel equations, using the refractive index data in Fig. 3a.

2.2. Frustrated external reflection

In both TIR and TER, light is incident on a material with a lower refractive index from a material with higher refractive index, at an angle greater than the critical angle, θ_{cr} (Fig. 1a-b). In both cases, the electric field just beyond the interface does not abruptly drop to zero, but decays exponentially as an evanescent wave [22]. When the lower-index material has a thickness on the order of the evanescent-wave decay length, light can tunnel through the material and emerge on the other side. This is referred to as frustrated total internal reflection (F-TIR) [23] [24] (Fig. 1c), and has numerous applications such as multi-touch sensing [23]. Analogously, this process can take place for external reflection, which we refer to as *frustrated external reflection* (F-ER; here we omit 'total' from the term due to the non-zero optical losses) (Fig. 1d).

We calculated the decay length of the evanescent wave [25] to approximately obtain the SiO_2 film thickness required for observation of F-ER (See the section 3 Supplementary Materials [14] for the calculation) [25]. To demonstrate F-ER experimentally, we deposited three SiO_2 films with thicknesses of 1.5, 3, and 6 μm onto double-side-polished high-resistivity silicon wafers using PECVD. At $\lambda_0 = 7.8\,\mu m$, these films have $\tilde{n}_{\mathrm{ox}} = 0.8 + 0.07i$ (Fig. 2), and thus $\theta_{cr} = 51°$. In Fig. 4a, we show the measured and calculated transmittance versus the incident angle for p polarization. The calculations were performed using the transfer-matrix method [26], assuming a silicon substrate thickness of 500 μm. The fine fringes in the

calculated data, which are due to thin-film interference in the silicon, are not observed in the experiment, most likely because of the non-zero numerical aperture (*i.e.*, each measurement corresponds to an average over a range of incident angles). The plotted calculated data was smoothed using a moving average to roughly emulate the measurement. Figure 4a shows that some light is transmitted even for $\theta > \theta_{\mathrm{cr}}$, demonstrating F-ER. As expected, an increase of the thickness of the SiO_2 layer (d) results in lower transmittance.

For $\theta > \theta_{\mathrm{cr}}$, the reflectance increases with increasing d (Fig. 4b), as the effect of frustration is reduced. For $\theta < \theta_{\mathrm{cr}}$, however, increasing d results in a decrease in reflectance. This occurs because $|\tilde{n}_{\mathrm{ox}}|$ is close to 1 (*i.e.*, the refractive index of air), so most of the reflected light comes from the SiO_2/Si interface rather than the air/SiO_2 interface. A thicker SiO_2 film absorbs more light, reducing the overall intensity that emerges back into the air. At angles beyond θ_{cr}, the slope of the transmittance vs. angle changes, indicating the onset of F-ER (see Fig. 4a). Note that the reflectance does not reach unity even at very oblique angles because of evanescent-wave absorption within the SiO_2 (*i.e.*, no *total* external reflection). See the Appendix 1 for more detailed calculations of a fictitious case with no optical absorption.

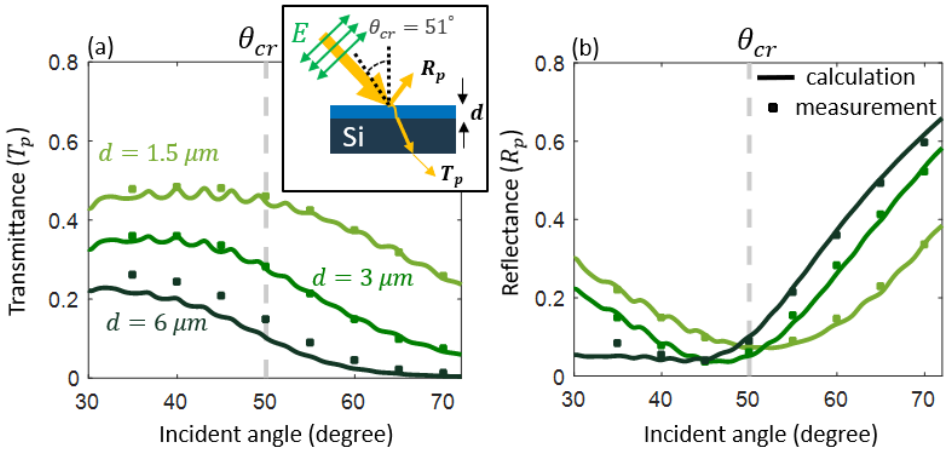

Figure 4) Frustration of external reflection

(a) Transmittance and **(b)** reflectance of an SiO_2 film on a silicon substrate, for p-polarized light versus incident angle at $\lambda_0 = 7.8\ \mu m$, for three different film thicknesses of SiO_2, d. The $d = 6\ \mu$m film is significantly thicker than the evanescent decay length δ, so almost no light is transmitted for incident angles beyond θ_{cr}, maximizing reflectance. Conversely, for the thinner films, the transmittance does not drop completely to zero, and the reflectance is reduced, indicating frustrated external reflection (F-ER). θ_{cr} is identified with a vertical dashed grey line.

2.3. Direct coupling to surface plasmon waves from air

The use of materials with $n < 1$ allows us to "invert" many common configurations in optics, using air as a high-index medium (Fig. 1). To demonstrate the generality of this concept, we explored replacing the high-index prism in the well-known Kretschmann configuration for coupling to surface-plasmon polaritons

(SPPs) [27] with air. Specifically, we explore coupling to SPPs at the interface between gold (Au) and SiO_2, in the 7.4 – 7.7 μm wavelength region, where $n_{ox} < 1$ and $\kappa_{ox} < 0.08$ (Fig. 2).

Our simple structure comprises roughly 10 nm of evaporated Au on top of an SiO_2 wafer (Fig. 5a). Using the transfer-matrix method, we calculated angle-dependent reflectance from air for slightly different wavelengths (7.45, 7.56, and 7.67 μm) corresponding to different values of n_{ox} (0.9, 0.84, and 0.76, respectively) (Fig. 5a). The local minima in reflectance are evidence of coupling to SPPs propagating along the SiO_2/Au interface. The positions of these minima shift toward smaller incident angles for increasing wavelength, as expected from the dispersion of SiO_2 (Fig. 2a), and the minima become deeper for thinner films (see Appendix 2). Figure 5b shows the corresponding experimental results, which are in good agreement with our calculations.

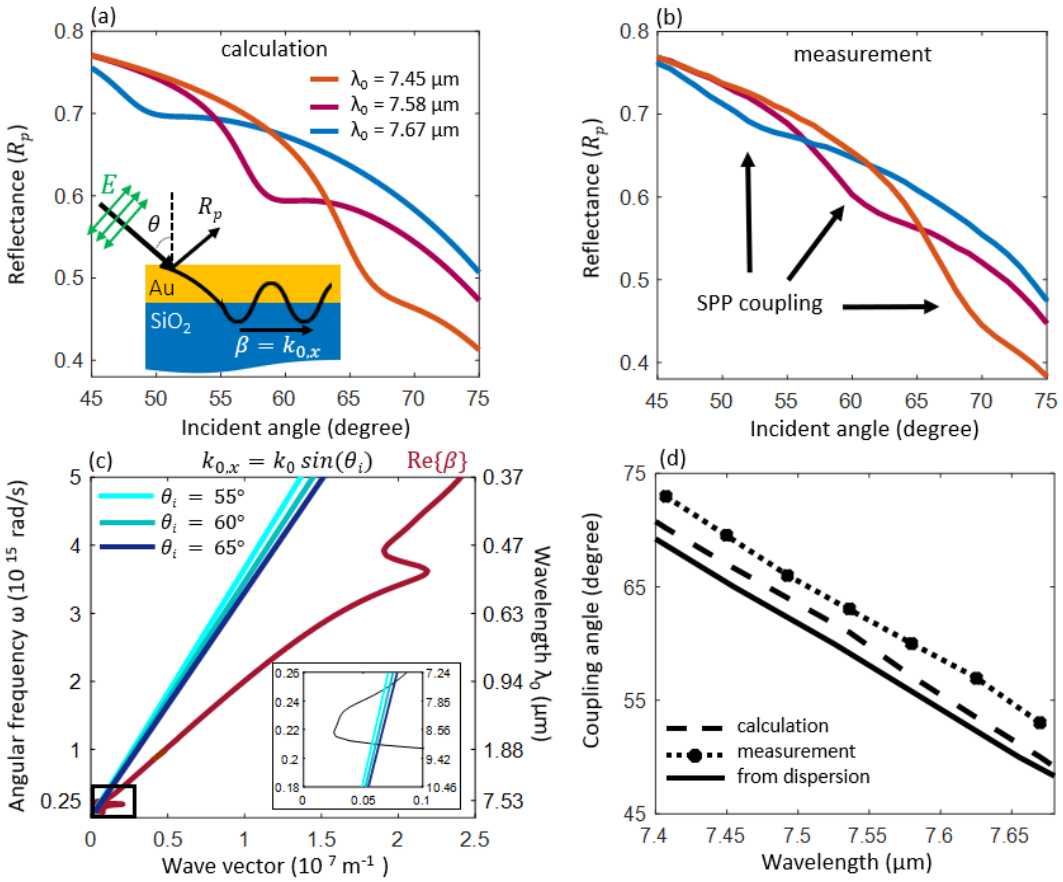

Figure 5) Direct coupling to SPPs from free space

(a) Calculated and **(b)** measured p-polarized angle-dependent reflectance of a ~10 nm Au film deposited on an SiO_2 substrate at $\lambda_0 = 7.45, 7.58,$ and $7.67\ \mu m$, corresponding to $n_{ox} = 0.9, 0.84,$ and 0.76, respectively. The dips are evidence of coupling to SPPs at the interface between Au and SiO_2. **(c)** Dispersion plots for incident light for different angles, and SPPs at the Au/SiO_2 interface. The intersections around 7.5 μm (see inset) correspond to locations of the dips in the reflectance curves in (a, b). Three blue traces show $k_{0,x}$, the x-component of the wave vector of the incident light, for $\theta_i = 55, 60, 65$ °. Smaller angles of incidence correspond to smaller $k_{0,x}$, and therefore intersections of $k_{0,x}$ and β occur at lower frequency and longer wavelength. **d)** Summary of the results in parts (a-b) and (c). The dashed

and dotted lines identify the angular positions of the dips in the reflectance curves from (a) and (b). The black solid line corresponds to the intersections between the dispersion curves in (c), signifying coupling to SPPs.

To verify that these minima in reflectance correspond to coupling to SPPs, we plotted the dispersion relation of single-interface SPPs [28] and the dispersion curves of the incident light — taking only the component of the incident wave vector along the interface — for several different incidence angles (Fig. 5c). Direct coupling to SPPs is expected to occur roughly where these curves intersect. It can be seen in the inset of Fig. 5c, which zooms in on the region where $n_{\mathrm{ox}} < 1$, that for every angle there are two distinct intersections. Only the shorter-wavelength intersection ($\sim 7.5\ \mu m$) results in clear coupling to SPPs. The wavelength of the other intersection ($\sim 9\ \mu m$) corresponds to high losses in the SiO_2 (Fig. 2b), so the SPPs are almost immediately absorbed (more information about the other intersection and the propagation length of SPPs can be found in section 6 of Supplementary Materials [14]). In Fig. 5d, we converted the intersections in the dispersion to a plot of the predicted coupling angle versus free-space wavelength (solid line). This curve matches well with the actual measured and calculated coupling angles. The slight discrepancy may be a result of experimental uncertainty and the limitations of the SPP wave-vector equation, which assumes that both the metal and dielectric have semi-infinite thickness [28].

2.4. Other materials

The phenomena described in this paper all become easier to observe for materials that simultaneously have n significantly below 1 and minimal losses. However, the frequency dependences of n and κ are always connected (as described by the Kramers-Kronig relations [29]) and generally have an inverse relationship; *e.g.*, the reduction of n in SiO_2 is accompanied by an increase of κ on the lower-loss side of the resonance (Fig. 2). To evaluate candidate materials, we define a figure of merit that simultaneously quantifies the loss and the difference of n from unity: $\eta = \kappa/(1-n)$. This figure of merit is used in the X-ray regime to quantify the sharpness of the transition between ordinary and external reflection [30] (more discussion in Appendix 3). In Fig. 6, we plotted η as a function of frequency in the near and mid infrared for several candidate materials with optical-phonon or plasma resonances [11], [31]. Among the materials we explored, silicon carbide reaches the smallest value of η [32], and lithium fluoride has the longest wavelength span for which $n < 1$ and $\eta < 1$ [33]. In general, fluorides seem to be good candidate materials [34], with the wavelength of the $n < 1$ region increasing for larger cations. We note that many of these candidate

materials are transparent with $n > 1$ at shorter wavelengths (*e.g.*, in the visible), potentially enabling very different functionalities in different spectral ranges.

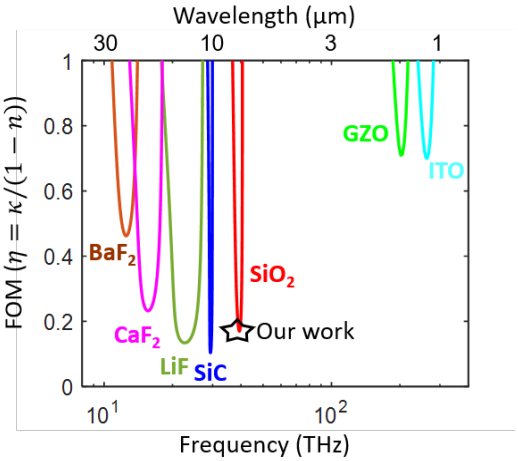

Figure 6) Figure of merit, $\eta = \kappa/(1-n)$, for several candidate materials with $n < 1$, including transparent conducting oxides in the near infrared and dielectric materials with strong phonon resonances in the mid infrared (material data from refs. [11], [31], [32], [33], and [34].)

3. Conclusion

In this article, we explored the use of low-loss materials with refractive index below unity ($n < 1$) to "invert" several well-known configurations in optics that are based on total or attenuated internal reflection. We showed that transparent dielectrics in visible range, with strong phonon resonances at mid-infrared frequencies are good candidate materials for such applications, experimentally demonstrating *external reflection*, *frustrated external reflection*, and *direct coupling to surface plasmon polaritons* from free space without using prisms or surface modulation. We envision potential applications of the $n < 1$ region in these dielectrics and other materials with low-loss resonances for spectral or angular filtering, air-core waveguiding, cloaking, and surface-plasmon-based sensing.

Acknowledgements

We acknowledge funding from the Office of Naval Research (Grant No. N00014-16-1-2556) and UW Madison. BS acknowledges a Graduate Research Fellowship from the National Science Foundation. PJR acknowledges a Critical Skills Master's Fellowship from Sandia National Labs. We thank M. Shahabadi and R. Wambold for helpful discussions. The PECVD of SiO_2 was performed at the Harvard Center for Nanoscale Systems by P. de Rouffignac. Various characterization was performed at the Materials Science Center and Soft Materials Laboratory, core facilities at UW-Madison. The authors acknowledge use of facilities and instrumentation supported by NSF through the University of Wisconsin Materials Research Science and Engineering Center (DMR-1720415).

Appendix

1- Frustration of external reflection for lossless SiO_2

Figure 7 shows the calculation of reflection and transmission versus incident angle for the same structure of SiO_2 on top of silicon substrate as in Fig. 4, assuming there is no optical loss in the SiO_2 ($\kappa_{ox} = 0$), but the same n_{ox} as in the main text. This calculation was done to analyze frustrated *total* external reflection, and it shows that the transition to total reflection occurs much faster across the critical angle compared to the real case with optical loss. Similarly to the real case with losses, the transition happens more gradually for thinner films. Note that there exists an angle in both the angular reflection and transmission plots at which the curves for different thickness overlap; this corresponds to the Brewster angle at the SiO_2/Si interface. At this angle, the reflection from the structure is dominated by the air/SiO_2 interface; therefore, reflection becomes independent of the film thickness.

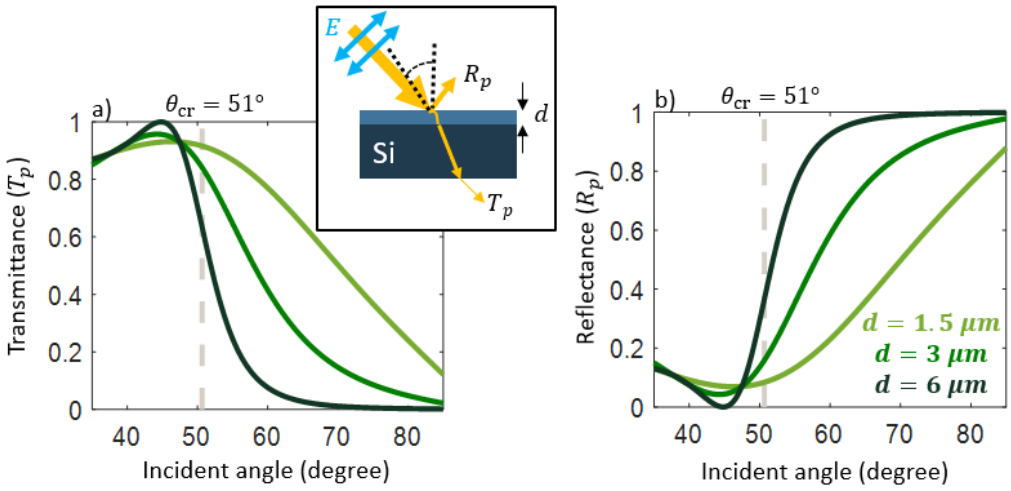

Figure 7) (a) Transmittance and (b) reflectance of a fictitious SiO_2 film without optical loss on a silicon substrate, for p-polarized light, versus incident angle at $\lambda_0 = 7.8\ \mu m$, for three different film thicknesses of SiO_2, *d*. θ_{cr} is identified with a vertical grey line.

2- Effect of gold thickness on direct SPP coupling

In this section, we examine the effect of the gold thickness, d, on the coupling between free-space light and SPPs on the Au/SiO_2 interface of the structure in Fig. 5. In Fig. 8, we show the calculation performed for Fig. 5(a), but for several values of *d*. By decreasing d, the dips corresponding to coupling to SPPs become deeper. Critical coupling appears to be reached for $d \sim 2$ nm, indicating that for $d = 10$ nm the system is heavily undercoupled; this explains why the dips in Fig. 5(a, b) are so shallow.

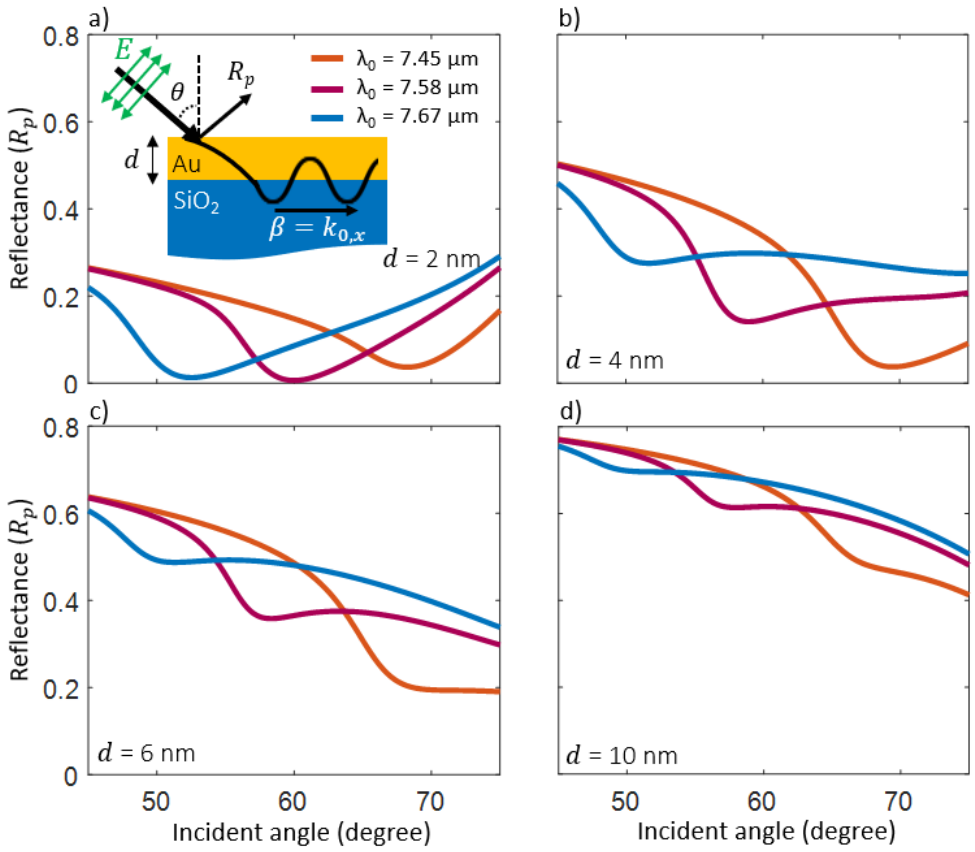

Figure 8) Effect of gold-layer thickness, d, on direct coupling to SPPs for (a) $d = 2$ nm, (b) $d = 4$ nm, (c) $d = 6$ nm, and (d) $d = 10$ nm. Note that (d) displays the same data as Fig. 5(a).

3- Transition to total external reflection

In this section, the reflection of light at an interface between air and a material with $n < 1$ for different polarizations of light versus incident angle is shown. In Fig. 9(a, b), it is assumed that n is constant and smaller than one (in this case, 0.7), and κ varies. These plots show that a sharper transition to external reflection can be achieved by using a material with lower loss.

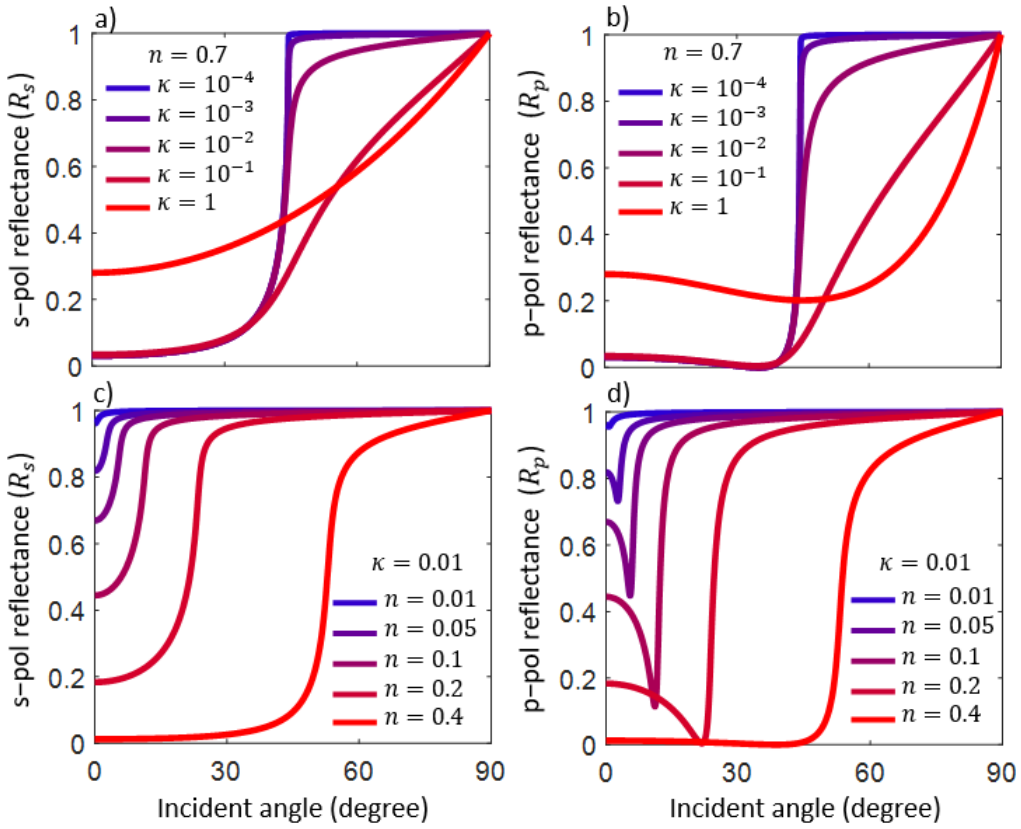

Figure 9) Transition to total external reflection with various values of n and κ

(a,b) The increase of optical loss (κ) smooths the transition to total reflection. (c, d) Change of refractive index (n) changes the critical angle.

Setting a constant κ for the material with $n < 1$ and sweeping n results in different critical angles of external reflection (Fig. 9(c, d)). Also, increasing n results in a more gradual transition. To consider the effect of both n and κ, we used a figure of merit, $\eta = \kappa/(1-n)$, used at X-ray frequencies [30]. A decrease of η results in a sharper transition to total external reflection. In Fig. 10, we plot the polarization-averaged reflection of several materials from Fig. 6, versus the incident angle divided by the critical angle, at the wavelengths at which η is minimum.

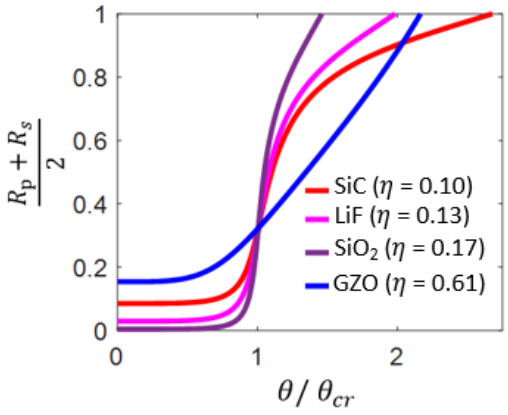

Figure 10) Polarization-averaged reflectance versus incident angle, normalized to the critical angle, for several representative materials from Fig. 6. Each plot is at the wavelength for which η is minimum for that material.

References

[1] E. D. Palik, Handbook of optical constants of solids, 3. Academic Press (1998).

[2] A. Sihvola, Metamaterials in electromagnetics, Metamaterials **1**, 2 (2007).

[3] V. G. Veselago, The Electrodynamics of Substances With Simultaneously Negative Values of ε and μ, Sov. Phys. uspekhi **10**, 509 (1968).

[4] J. B. Pendry, Negative refraction makes a perfect lens, Phys. Rev. Lett. **85**, 3966 (2000).

[5] R. A. Shelby, D. R. Smith, and S. Schultz, Experimental Verification of a Negative Index of Refraction, Science **292**, 77 (2001).

[6] N. Engheta, Tunneling of Electromagnetic Energy through Subwavelength Channels and Bends using ε-Near-Zero Materials, Phys. Rev. Lett., **157403**, 1 (2006).

[7] I. Liberal and N. Engheta, Near-zero refractive index photonics, Nat. Photonics, **11**, 149 (2017).

[8] M. G. Silveirinha and N. Engheta, Theory of supercoupling, squeezing wave energy, and field confinement in narrow channels and tight bends using ε near-zero metamaterials, Phys. Rev. B, **76**, 245109 (2007).

[9] J. B. Khurgin, How to deal with the loss in plasmonics and metamaterials, Nat. Nanotechnol., **10**, 2 (2015).

[10] A. Y. Zhu et al., Traditional and emerging materials for optical metasurfaces, Nanophotonics, **6**,

452 (2017).

[11] F. Y. Kischkat J et al., Mid-infrared optical properties of thin films of aluminum oxide , titanium dioxide, silicon dioxide, aluminum nitride, and silicon nitride, Appl. Opt., **51,** 6789 (2012).

[12] J. D. Caldwell et al., Low-loss, infrared and terahertz nanophotonics using surface phonon polaritons, Nanophotonics, **4**, 44 (2015).

[13] H. G. Tompkins, E. A. Irene, C. Hill, and N. Carolina, Handbook of Ellipsometry, (2005).

[14] See Supplemental Material at []. Section 1 gives more information about the optical properties of silica, further discussion regarding pseudo-Brewster angle is provided at section 2, decay lengh calculation of silica is at section 3, and more information about optical loss of direct coupled SPPs is at section 4.

[15] B. T. Schwartz and R. Piestun, Total external reflection from metamaterials with ultralow refractive index, JOSA B, **20**, 2448 (2003).

[16] H. Mimura et al., Efficient focusing of hard x rays to by a total reflection mirror Efficient focusing of hard x rays to 25 nm by a total reflection mirror, Appl. Phys. Lett., **90,** 051903 (2007).

[17] G. E Ice, J. S. Chung, J.Z. Tischler, A. Lunt, and L. Assoufid, Elliptical x-ray microprobe mirrors by differential deposition Elliptical x-ray microprobe mirrors by differential deposition, Rev. Sci. Instrum., **71**, 2635 (2000).

[18] B. T. Schwartz and R. Piestun, Waveguiding in air by total external reflection from ultralow index metamaterials, Appl. Phys. Lett., **85**, 1 (2004).

[19] S. Babar and J. H. Weaver, Optical constants of Cu , Ag , and Au revisited, Appl. Opt., **54**, 477 (2015).

[20] M. Akimoto and Y. Gekka, Brewster and Pseudo-Brewster angle technique for determination of Optical Constants, Jpn. J. Appl. Phys., **1R**, 120 (1992).

[21] S. Y. Kim and K. Vedam, Analytic solution of the pseudo-Brewster angle, JOSA A, **3**, 1772 (1986).

[22] E. Hecht, Optics. Pearson Education, 2016.

[23] J. Y. Han, Low-cost multi-touch sensing through frustrated total internal reflection, Proc.18thAnnu. Symp. user interface Softw. Technol. - UIST ’05.ACM, pp. 115 (2005).

[24] S. Zhu, A.W. Yu, D. Hawley and R. Roy, Frustrated total internal reflection, Am. J. Phys., **54**, 601 (1986).

[25] A. R. Hind and A. M. Bhargava, Suresh K, At the solid/liquid interface: FTIR/ATR—the tool of

choice, Adv. Colloid Interface Sci., **93**, 91 (2001).

[26] S. J. Byrnes, Multilayer optical calculations, arXiv:1603.02720.

[27] E. Kretschmann, Die Bestimmung optischer Konstanten von Metallen durch Anregung von Oberfliichenplasmaschwingungen, Zeitschrift für Phys. A Hadron. Nucl., **241**, 313 (1971).

[28] W. L. Barnes, A. Dereux, and T. W. Ebbesen, Surface plasmon subwavelength optics, Nature, **424**, 824 (2003).

[29] E. M. Lucarini, V., Saarinen, J. J., Peiponen, K. E., & Vartiainen, Kramers-Kronig relations in optical materials research. Springer Science & Business Media, 2005.

[30] D. Attwood, Soft X-rays and Extreme Ultraviolet. 1999.

[31] J. Kim, G. V Naik, N. K. Emani, U. Guler, and A. Boltasseva, Plasmonic Resonances in Nanostructured Transparent Conducting Oxide Films, IEEE J. Sel. Top. Quantum Electron., **19**, 4601907 (2013).

[32] D. W. Spitzer, W. G., Kleinman, D., Infrared Properties of Hexagonal Silicon Carbide, Phys. Rev., **113**, 127 (1959).

[33] J. R. Jasperse, A. Kahan, J. N. Plendl, and S. S. Mitra, Temperature dependence of infrared dispersion in ionic crystals LiF and MgO, Phys. Rev., **146**, 526 (1966).

[34] L. E. Kaiser, W., Spitzer, W. G., Kaiser, R. H., & Howarth, Infrared Properties of CaF_2, SrF_2, and BaF_2, Phys. Rev., **127**, 1950 (1962).

[35] J. E. Olsen and F. Shimura, Infrared reflection spectroscopy of the SiO_2-silicon interface, J. Appl. Phys., **66**, 1353 (1989).

[36] R. L. Olmon et al., Optical dielectric function of gold, Phys. Rev. B, **86**, 1 (2012).